

Exploring the Influence of Cosmic Curvature on Large-Scale Structure Formation: Part I - Homogeneous Dark Energy Presence

Bikash R. Dinda ^{1,2,*}

¹*Department of Physical Sciences, Indian Institute of Science Education and Research Kolkata, Mohanpur, Nadia, West Bengal 741246, India.*

²*Department of Physics & Astronomy, University of the Western Cape, Cape Town, 7535, South Africa.*

This study explores the impact of cosmic curvature on structure formation through general relativistic first-order perturbation theory. We analyze continuity and Euler equations, incorporating cosmic curvature into Einstein equations. Emphasizing late-time dynamics, we investigate matter density contrast evolution in the presence of cosmic curvature, with a specific focus on sub-hubble scales. Solving the evolution equation, we conduct data analysis using cosmic chronometers, baryon acoustic oscillations, type Ia supernova observations and $f\sigma_8$ data. While constraints on some parameters remain consistent, excluding cosmic curvature tightens constraints on Ω_{m0} and σ_{80} in Λ CDM and w CDM models. Intriguingly, the non-phantom behavior of dark energy proves more favorable in both w CDM and CPL models across diverse data combinations.

PACS numbers:

I. INTRODUCTION

The investigation into the late-time cosmic dynamics by observations like type Ia supernovae [1–8], cosmic microwave background [9–11], baryon acoustic oscillations [12–14], and cosmic chronometers [15–17], has strongly established the accelerating expansion of our Universe. This cosmic acceleration, however, can not be explained within the standard matter or dark matter paradigms governed by general relativity. Consequently, two popular theoretical aspects have emerged to explain this late-time cosmic acceleration: the existence of dark energy [18–23] or the modifications to the general theory of relativity on cosmic scales [24–36]. While dark energy being a constituent of the Universe with large negative pressure, capable of driving the cosmic acceleration, alternative theories of modified gravity account for the observed cosmic acceleration without introducing any dark energy component.

Among different models of dark energy, arguably the Λ CDM model stands out as the most successful [37]. In this model, a cosmological constant (Λ), with a constant equation of state, with value -1 acts as a dark energy component. Despite its success, the Λ CDM model has some shortcomings. For example, from the theoretical perspective, issues like cosmic coincidence and fine-tuning problems [38–41] are present. Moreover, observational tensions, including the Hubble tension [42–45] and σ_8 (or S_8) tension [46–49] corresponding to the discrepan-

cies in measured values of H_0 and σ_{80} between early and late time observations. This necessitates studies of models beyond Λ CDM.

The standard Λ CDM model assumes that the 3-space of the four-dimensional space-time is flat [9–11]. However, it is important to incorporate the influence of cosmic curvature into our analysis to study its impact. While literature acknowledges prior investigations exploring the prospect of non-zero cosmic curvature in the Universe [50–70], these studies predominantly focus on the background dynamics of cosmic expansion due to the introduction of non-zero spatial curvature. Yet, it is crucial to examine the impact of cosmic curvature on the evolution of perturbations [71]. In this study, we go beyond the conventional approach by not only considering the effect of cosmic curvature on background dynamics but also delving into its role in shaping the evolution of first-order perturbations. This exploration involves crucial quantities like the matter density contrast and the growth rate.

Regarding the dynamical dark energy models beyond the Λ CDM, there are potential degeneracies between the equation of state for dark energy and cosmic curvature. This fact necessitates a comprehensive exploration of alternative dark energy models [72–76] with the presence of cosmic curvature. In this study, we go beyond the standard Λ CDM model and delve into dynamical dark energy models in the presence of cosmic curvature. Specifically, we consider the w CDM and the Chevallier-Polarski-Linder (CPL) [77, 78] model. The w CDM model features a dark energy equation of state that remains static over time but can take various values, including the cosmological constant's value of -1 .

*Electronic address: bikashrdinda@gmail.com

On the other hand, the CPL model introduces dynamic variations in the equation of state of dark energy. By adopting these models, we aim to scrutinize the potential degeneracies between the equation of state for dark energy and cosmic curvature and the implications of these in the cosmological dynamics.

While most of the studies often assume the homogeneity of dark energy, particularly evident in the Λ CDM model where dark energy exhibits no fluctuations, we incorporate these fluctuations in our study in the first place. Inclusion of these fluctuations on large scales is important even in dark energy models like w CDM and CPL [79–83]. Thus, these dark energy perturbations have the potential impact on large-scale structure formation [84–86]. To accomplish this, we study a robust mathematical framework that integrates dark energy perturbations within the framework of first-order general relativistic perturbation theory. It is essential to note that while the theoretical derivation is carried out in this part of the study, the actual data analysis, focusing on realistic dark energy models such as quintessence and k -essence featuring fluctuations, will be investigated in the subsequent section of our research.

This paper is structured as follows. Sec. II delves into the metric employed for the first-order general relativistic perturbation theory, focusing on scalar fluctuations excluding anisotropic stress. In Sec. III, we compute the background and first-order Einstein tensor components within this metric. The evolution of the perfect fluid in both background and first-order perturbation, including velocity fields, energy-momentum tensor, continuity, and Euler equations, is detailed in Sec. IV. Sec. V concentrates on treating matter as a perfect fluid, deriving continuity and Euler equations, and establishing a differential equation for the matter density contrast. Late-time dynamics, exploring background expansion and scalar perturbation evolution with matter and dark energy have been discussed in Sec. VI. Sec. VII reformulates all evolution equations in the sub-Hubble limit for computational simplicity and to extract relevant perturbation quantities like the growth rate. The four observational datasets considered in this analysis are briefly outlined in Sec. VIII. Sec. IX delves into the main study findings. Finally, in Sec. X we present a conclusion.

II. THE METRIC TO DESCRIBE BACKGROUND AND FIRST-ORDER SCALAR FLUCTUATIONS

We adopt the conformal Newtonian gauge to study the first-order general relativistic perturbations. Within

this gauge, the line element, denoted as d_s , characterizing solely scalar fluctuations, is expressed as

$$d_s^2 = \sigma \left[-c^2(1 + 2\Phi)dt^2 + a^2(1 - 2\Phi) \left(\frac{dr^2}{1 - \kappa r^2} + r^2 d\theta^2 + r^2 \sin^2 \theta d\phi^2 \right) \right], \quad (1)$$

where t represents cosmic time, r denotes the comoving radial coordinate, and θ and ϕ stand for the comoving polar and azimuthal angles, respectively. κ signifies the curvature of space-time, while c is the speed of light in a vacuum and a is the cosmic scale factor. The Bardeen potential is denoted as Φ , and the parameter σ is introduced to characterize the signature of the metric in the line element, defined as

$$\sigma = \begin{cases} +1, & \text{for } (-, +, +, +) \text{ signature,} \\ -1, & \text{for } (+, -, -, -) \text{ signature.} \end{cases} \quad (2)$$

Note that in the line element given by Eq. (1), we adopt the scalar-vector-tensor decomposition theory. This allows us to analyze scalar fluctuations independently. Additionally, our assumption of the absence of anisotropic stresses enables us to focus on a single degree of freedom in the scalar fluctuations, governed by the Bardeen potential Φ . A background metric, representing the Friedmann-Lemaître-Robertson-Walker (FLRW) metric with curvature contributions, is characterized by $\Phi = 0$.

The metric and its inverse can be expressed perturbatively as follows

$$g_{\mu\nu} = \bar{g}_{\mu\nu} + \delta g_{\mu\nu}, \quad (3)$$

$$g^{\mu\nu} = \bar{g}^{\mu\nu} + \delta g^{\mu\nu}, \quad (4)$$

respectively. We denote the background counterpart of a quantity with an over bar, and its first-order perturbation with the pre-factor δ . Consistent notation is maintained throughout this study. The non-zero components of both the background metric and its inverse are listed below:

$$\bar{g}_{tt} = -\sigma c^2, \quad \bar{g}_{rr} = \frac{\sigma a^2}{1 - \kappa r^2}, \quad \bar{g}_{\theta\theta} = \sigma a^2 r^2, \quad \bar{g}_{\phi\phi} = \sigma a^2 r^2 \sin^2 \theta, \quad (5)$$

$$\bar{g}^{tt} = -\frac{\sigma}{c^2}, \quad \bar{g}^{rr} = \frac{\sigma(1 - \kappa r^2)}{a^2}, \quad \bar{g}^{\theta\theta} = \frac{\sigma}{a^2 r^2}, \quad \bar{g}^{\phi\phi} = \frac{\sigma}{a^2 r^2 \sin^2 \theta}. \quad (6)$$

The non-zero components of the first-order metric and its inverse are listed below:

$$\begin{aligned} \delta g_{tt} &= -2\sigma c^2 \Phi, \quad \delta g_{rr} = -\frac{2\sigma a^2 \Phi}{1 - \kappa r^2}, \quad \delta g_{\theta\theta} = -2\sigma a^2 r^2 \Phi, \\ \delta g_{\phi\phi} &= -2\sigma a^2 r^2 (\sin^2 \theta) \Phi, \\ \delta g^{tt} &= \frac{2\sigma \Phi}{c^2}, \quad \delta g^{rr} = \frac{2\sigma(1 - \kappa r^2)\Phi}{a^2}, \quad \delta g^{\theta\theta} = \frac{2\sigma \Phi}{a^2 r^2}, \\ \delta g^{\phi\phi} &= \frac{2\sigma \Phi}{a^2 r^2 \sin^2 \theta}. \end{aligned} \quad (7)$$

III. THE BACKGROUND AND THE FIRST ORDER EINSTEIN TENSOR

With the components of the metric and its inverse in hand, we proceed to compute the components of the Einstein tensor perturbatively, denoted as

$$G_\nu^\mu = \bar{G}_\nu^\mu + \delta G_\nu^\mu. \quad (9)$$

The non-zero components of the Einstein tensor are provided below:

$$\bar{G}_t^t = -3\sigma \left(\frac{H^2}{c^2} + \frac{\kappa}{a^2} \right), \quad (10)$$

$$\bar{G}_r^r = \bar{G}_\theta^\theta = \bar{G}_\phi^\phi = -\sigma \left(\frac{2\dot{H} + 3H^2}{c^2} + \frac{\kappa}{a^2} \right), \quad (11)$$

where an over dot on a quantity indicates the partial derivative of that quantity w.r.t cosmic time t . It's important to note that for background quantities, the partial derivative w.r.t t is equivalent to the total derivative w.r.t t because all background quantities are functions of cosmic time t . On the other hand, perturbed quantities are functions of all four coordinates— t , r , θ , and ϕ . Here, H represents the Hubble parameter, defined as $\frac{\dot{a}}{a}$. The t - t component of the first-order Einstein tensor is expressed as

$$\delta G_t^t = 2\sigma \left[\frac{3H \left(\frac{\partial \Phi}{\partial t} + H\Phi \right)}{c^2} - \frac{\vec{\nabla}^2 \Phi + 3\kappa \Phi}{a^2} \right], \quad (12)$$

where $\vec{\nabla}^2 f$ represents the comoving gradient square, corresponding to the three-dimensional space, of a quantity f , and is defined as

$$\begin{aligned} \vec{\nabla}^2 f &= \frac{1}{h_r h_\theta h_\phi} \left[\frac{\partial}{\partial r} \left(\frac{h_\theta h_\phi}{h_r} \frac{\partial f}{\partial r} \right) + \frac{\partial}{\partial \theta} \left(\frac{h_\phi h_r}{h_\theta} \frac{\partial f}{\partial \theta} \right) \right. \\ &\quad \left. + \frac{\partial}{\partial \phi} \left(\frac{h_r h_\theta}{h_\phi} \frac{\partial f}{\partial \phi} \right) \right], \\ &= \frac{1}{r^2} \left[r^2(1 - \kappa r^2) \frac{\partial^2 v}{\partial r^2} + r(2 - 3\kappa r^2) \frac{\partial f}{\partial r} + \frac{\partial^2 v}{\partial \theta^2} \right. \\ &\quad \left. + (\cot \theta) \frac{\partial f}{\partial \theta} + \frac{\partial^2 f}{\sin^2 \theta} \right]. \end{aligned} \quad (13)$$

Here, the factors of the curvilinear coordinates are given as

$$\begin{aligned} h_r &= \frac{1}{\sqrt{1 - \kappa r^2}}, \\ h_\theta &= r, \\ h_\phi &= r \sin \theta. \end{aligned} \quad (14)$$

The r - t and t - r components of the first-order Einstein tensor are given as

$$\begin{aligned} \delta G_t^r &= \frac{2\sigma(1 - \kappa r^2)}{a^2} \frac{\partial}{\partial r} \left(\frac{\partial \Phi}{\partial t} + H\Phi \right) \\ &= -\frac{c^2(1 - \kappa r^2)}{a^2} \delta G_r^t. \end{aligned} \quad (15)$$

The θ - t and t - θ components of the first-order Einstein tensor are given as

$$\delta G_t^\theta = \frac{2\sigma}{a^2 r^2} \frac{\partial}{\partial \theta} \left(\frac{\partial \Phi}{\partial t} + H\Phi \right) = -\frac{c^2}{a^2 r^2} \delta G_\theta^t. \quad (16)$$

The ϕ - t and t - ϕ components of the first-order Einstein tensor are given as

$$\begin{aligned} \delta G_t^\phi &= \frac{2\sigma}{a^2 r^2 \sin^2 \theta} \frac{\partial}{\partial \phi} \left(\frac{\partial \Phi}{\partial t} + H\Phi \right) \\ &= -\frac{c^2}{a^2 r^2 \sin^2 \theta} \delta G_\phi^t. \end{aligned} \quad (17)$$

The r - r , θ - θ , and ϕ - ϕ components of the first-order Einstein tensor are given as

$$\begin{aligned} \delta G_r^r &= \delta G_\theta^\theta = \delta G_\phi^\phi \\ &= 2\sigma \left[\frac{\frac{\partial^2 \Phi}{\partial t^2} + 4H \frac{\partial \Phi}{\partial t} + (2\dot{H} + 3H^2)\Phi}{c^2} - \frac{\kappa \Phi}{a^2} \right], \end{aligned} \quad (18)$$

All other components of the first-order Einstein tensor are trivially zero.

IV. THE DESCRIPTION OF A PERFECT FLUID

In this section, we elucidate the dynamics of a perfect fluid within this metric framework.

A. The background and the first order velocity field of a perfect fluid

To characterize a perfect fluid, let's express its four-velocity components, both covariant and contravariant, perturbatively as

$$U^\mu = \bar{U}^\mu + \delta U^\mu, \quad (19)$$

$$U_\mu = \bar{U}_\mu + \delta U_\mu. \quad (20)$$

The spatial components of the contravariant four-velocity become zero when studying only scalar fluctuations. Thus, we have

$$\bar{U}^r = \bar{U}^\theta = \bar{U}^\phi = 0. \quad (21)$$

The time component of the contravariant four-velocity can be computed using the identity provided as

$$\bar{g}_{\mu\nu}\bar{U}^\mu\bar{U}^\nu = -\sigma c^2. \quad (22)$$

Applying this identity, we derive an algebraic equation for \bar{U}^t as

$$(\bar{U}^t)^2 = 1, \quad (23)$$

and we opt for the positive solution of the above equation, yielding

$$\bar{U}^t = 1. \quad (24)$$

Utilizing the contraction with the background metric, i.e., $\bar{U}_\mu = \bar{g}_{\mu\nu}\bar{U}^\nu$, we obtain all components of the covariant four-velocity as

$$\bar{U}_t = -\sigma c^2, \quad \bar{U}_r = \bar{U}_\theta = \bar{U}_\phi = 0. \quad (25)$$

Similarly, the first-order time component of the contravariant four-vector is computed using the provided identity

$$g_{\mu\nu}U^\mu U^\nu = -\sigma c^2. \quad (26)$$

And we have

$$\delta U^t = -\Phi, \quad (27)$$

By using $U_\mu = g_{\mu\nu}U^\nu$, we get

$$\delta U_t = -\sigma c^2 \Phi, \quad (28)$$

$$\begin{aligned} \delta U_r &= \frac{\sigma a^2 \delta U^r}{1 - \kappa r^2}, \quad \delta U_\theta = \sigma a^2 r^2 \delta U^\theta, \\ \delta U_\phi &= \sigma a^2 r^2 (\sin^2 \theta) \delta U^\phi. \end{aligned} \quad (29)$$

The curl-free part of the velocity contributes to the scalar fluctuations. Therefore, we opt for

$$\begin{aligned} \delta U_r &= -\sigma \frac{\partial(av)}{\partial r}, \quad \delta U_\theta = -\sigma \frac{\partial(av)}{\partial \theta}, \\ \delta U_\phi &= -\sigma \frac{\partial(av)}{\partial \phi}. \end{aligned} \quad (30)$$

Now, employing the relations in Eq. (29), we determine the contravariant spatial components of the four-velocity as

$$\begin{aligned} \delta U^r &= -\frac{1 - \kappa r^2}{a} \frac{\partial v}{\partial r}, \quad \delta U^\theta = -\frac{1}{ar^2} \frac{\partial v}{\partial \theta}, \\ \delta U^\phi &= -\frac{1}{ar^2 \sin^2 \theta} \frac{\partial v}{\partial \phi}. \end{aligned} \quad (31)$$

B. The energy-momentum tensor of a perfect fluid

The energy-momentum tensor of a perfect fluid can be expressed in the following form

$$T_\nu^\mu = \left(\rho + \frac{P}{c^2} \right) U^\mu U_\nu + \sigma P \delta_\nu^\mu, \quad (32)$$

where ρ and P represent the volumetric mass density and pressure of the perfect fluid, respectively, while δ denotes the usual Kronecker delta symbol. Note that,

this δ is different from the previously used δ in front of any quantity. The volumetric mass density and pressure of the perfect fluid are expressed in perturbative order as

$$\rho = \bar{\rho} + \delta\rho, \quad (33)$$

$$P = \bar{P} + \delta P, \quad (34)$$

respectively. Similarly, the energy-momentum tensor of the perfect fluid can be expressed in perturbative order as

$$T_\nu^\mu = \bar{T}_\nu^\mu + \delta T_\nu^\mu, \quad (35)$$

Utilizing Eqs. (21), (24), (25), (27), (28), (31), (33), and (34) in Eq.(32), we obtain components of the energy-momentum tensor for both the background and first-order counterpart. The non-zero background components of the energy-momentum tensor for the perfect fluid are listed below

$$\bar{T}_t^t = -\sigma c^2 \bar{\rho}, \quad (36)$$

$$\bar{T}_r^r = \bar{T}_\theta^\theta = \bar{T}_\phi^\phi = \sigma \bar{P}. \quad (37)$$

The t - t component of the first-order energy-momentum tensor for the perfect fluid is given below

$$\delta T_t^t = -\sigma c^2 \delta\rho. \quad (38)$$

The r - t and t - r components of the first-order energy-momentum tensor for the perfect fluid are given below

$$\delta T_t^r = \frac{\sigma(1 - \kappa r^2)(c^2 \bar{\rho} + \bar{P}) \frac{\partial v}{\partial r}}{a} = -\frac{c^2(1 - \kappa r^2)}{a^2} \delta T_r^t. \quad (39)$$

The θ - t and t - θ components of the first-order energy-momentum tensor for the perfect fluid are given below

$$\delta T_t^\theta = \frac{\sigma(c^2 \bar{\rho} + \bar{P}) \frac{\partial v}{\partial \theta}}{a r^2} = -\frac{c^2}{a^2 r^2} \delta T_\theta^t. \quad (40)$$

The ϕ - t and t - ϕ components of the first-order energy-momentum tensor for the perfect fluid are given below

$$\delta T_t^\phi = \frac{\sigma(c^2 \bar{\rho} + \bar{P}) \frac{\partial v}{\partial \phi}}{a r^2 \sin^2 \theta} = -\frac{c^2}{a^2 r^2 \sin^2 \theta} \delta T_\phi^t, \quad (41)$$

The r - r , θ - θ , and ϕ - ϕ components of the first-order energy-momentum tensor for the perfect fluid are given below

$$\delta T_r^r = \delta T_\theta^\theta = \delta T_\phi^\phi = \sigma \delta P. \quad (42)$$

All other components of the first-order energy-momentum tensor for the perfect fluid are trivially zero.

C. The continuity equation for a perfect fluid

In this study, we assume that there is no interaction of the perfect fluid with other fields or fluids present in the universe. Therefore, the divergence of the energy-momentum tensor for the perfect fluid is zero, i.e.,

$$\nabla_\mu T_\nu^\mu = 0. \quad (43)$$

Analyzing the above equation order by order, we arrive at the background condition

$$\bar{\nabla}_\mu \bar{T}_\nu^\mu = 0. \quad (44)$$

The above condition corresponds to four equations. The t part of this equation corresponds to

$$\dot{\bar{\rho}} + 3H \left(\bar{\rho} + \frac{\bar{P}}{c^2} \right) = 0. \quad (45)$$

This constitutes the continuity equation for the perfect fluid at the background level. Now, we establish a relationship between the background pressure and energy density of the perfect fluid using a quantity called the equation of state, denoted by w and defined as

$$\bar{P} = w \bar{\rho} c^2. \quad (46)$$

Utilizing Eq.(46), Eq.(45) can be rewritten as

$$\dot{\bar{\rho}} + 3H(1 + w)\bar{\rho} = 0. \quad (47)$$

Similarly, we obtain the first-order continuity equation for the perfect fluid as

$$(\dot{\delta\rho}) + 3H \left(\delta\rho + \frac{\delta P}{c^2} \right) - \frac{(1+w)\bar{\rho}(\theta_g + 3a\dot{\Phi})}{a} = 0, \quad (48)$$

where

$$\begin{aligned} \theta_g = \vec{\nabla}^2 v = & \frac{1}{r^2} \left[r^2(1 - \kappa r^2) \frac{\partial^2 v}{\partial r^2} + r(2 - 3\kappa r^2) \frac{\partial v}{\partial r} \right. \\ & \left. + \frac{\partial^2 v}{\partial \theta^2} + (\cot \theta) \frac{\partial v}{\partial \theta} + \frac{\frac{\partial^2 v}{\partial \phi^2}}{\sin^2 \theta} \right]. \quad (49) \end{aligned}$$

Now, we define the density contrast, δ_g , for the perfect fluid as

$$\delta\rho = \bar{\rho}\delta_g. \quad (50)$$

Applying the above definition, Eq.(48) can be rewritten as

$$\dot{\delta}_g - 3wH\delta_g - \frac{(1+w)\theta_g}{a} - 3(1+w)\dot{\Phi} + \frac{3H(\delta P)}{c^2\bar{\rho}} = 0. \quad (51)$$

D. The Euler equations for a perfect fluid

The spatial parts of Eq.(43) are referred to as the Euler equations for the perfect fluid. The background Euler equations for the perfect fluid are trivially zero, i.e.,

$$\bar{\nabla}_\mu \bar{T}_r^\mu = \bar{\nabla}_\mu \bar{T}_\theta^\mu = \bar{\nabla}_\mu \bar{T}_\phi^\mu = 0. \quad (52)$$

So, we do not obtain any corresponding equations. The first-order Euler equations corresponding to the conditions $\nabla_\mu T_r^\mu = 0$, $\nabla_\mu T_\theta^\mu = 0$, and $\nabla_\mu T_\phi^\mu = 0$ are given as

$$\frac{\partial A}{\partial r} = 0, \quad (53)$$

$$\frac{\partial A}{\partial \theta} = 0, \quad (54)$$

$$\frac{\partial A}{\partial \phi} = 0, \quad (55)$$

respectively, where we have

$$A = \dot{v} + \left[(1 - 3w)H + \frac{\dot{w}}{1+w} \right] v - \frac{c^2\Phi}{a} - \frac{\delta P}{a(1+w)\bar{\rho}}. \quad (56)$$

As all three spatial first derivatives of A are individually zero, we can further manipulate these equations into the following form to obtain a single useful Euler equation given as

$$\begin{aligned} & \frac{1}{h_r h_\theta h_\phi} \left[\frac{\partial}{\partial r} \left(\frac{h_\theta h_\phi}{h_r} \frac{\partial A}{\partial r} \right) + \frac{\partial}{\partial \theta} \left(\frac{h_\phi h_r}{h_\theta} \frac{\partial A}{\partial \theta} \right) \right. \\ & \left. + \frac{\partial}{\partial \phi} \left(\frac{h_r h_\theta}{h_\phi} \frac{\partial A}{\partial \phi} \right) \right] = \vec{\nabla}^2 A = 0. \quad (57) \end{aligned}$$

Finally, by substituting the expression of A from Eq.(56) into Eq.(57), we obtain a simplified form of the Euler equation for the perfect fluid given as

$$\begin{aligned} & \dot{\theta}_g + \left[(1 - 3w)H + \frac{\dot{w}}{1+w} \right] \theta_g - \frac{c^2\vec{\nabla}^2\Phi}{a} \\ & - \frac{\vec{\nabla}^2(\delta P)}{a(1+w)\bar{\rho}} = 0. \quad (58) \end{aligned}$$

V. MATTER AS A PERFECT FLUID

The matter components of the Universe can be modeled as a perfect fluid. In this context, we assume the matter is cold, implying zero background Pressure, resulting in an equation of state $w = 0$, and also, first-order pressure is zero for the matter. Additionally, we assume that matter does not interact with other fields. Because matter is considered a perfect fluid, all the equations describing a perfect fluid hold for the matter, with the additional constraints $w = 0$, $\bar{P} = 0$, and $\delta P = 0$. Moreover, $\dot{w} = 0$ and $\vec{\nabla}^2(\delta P) = 0$. Throughout this study, we denote all non-zero quantities related to matter with the subscript "m". Using these considerations, let's outline the key equations for the matter counterpart. By substituting $w = 0$ into Eq.(47), we obtain the background continuity equation for matter given as

$$\dot{\bar{\rho}}_m + 3H\bar{\rho}_m = 0. \quad (59)$$

Similarly, substituting $w = 0$ and $\delta P = 0$ into Eq.(51), we derive the first-order continuity equation for matter given as

$$\dot{\delta}_m - \frac{\theta_m}{a} - 3\dot{\Phi} = 0. \quad (60)$$

Similarly, substituting $w = 0$, $\dot{w} = 0$, and $\vec{\nabla}^2(\delta P) = 0$ into Eq.(58), we derive the first-order Euler equation for matter given as

$$\dot{\theta}_m + H\theta_m - \frac{c^2\vec{\nabla}^2\Phi}{a} = 0. \quad (61)$$

Let's further manipulate Eqs.(60) and (61) to derive a more useful differential equation for the matter. To do this, we first take the time derivative of Eq.(60), resulting in

$$\ddot{\delta}_m - \frac{\dot{\theta}_m}{a} + \frac{H\theta_m}{a} - 3\ddot{\Phi} = 0. \quad (62)$$

By utilizing Eq.(61), we obtain

$$\dot{\theta}_m = \frac{c^2\vec{\nabla}^2\Phi}{a} - H\theta_m. \quad (63)$$

Substituting the above equation into Eq.(62), we obtain

$$\ddot{\delta}_m + \frac{2H\theta_m}{a} - \frac{c^2\vec{\nabla}^2\Phi}{a^2} - 3\ddot{\Phi} = 0. \quad (64)$$

By employing Eq.(60), we obtain

$$\theta_m = a(\dot{\delta}_m - 3\dot{\Phi}). \quad (65)$$

Substituting the above equation into Eq.(64), we obtain a second-order differential equation for δ_m that is independent of θ_m , given as

$$\ddot{\delta}_m + 2H\dot{\delta}_m - \frac{c^2\vec{\nabla}^2\Phi}{a^2} - 6H\dot{\Phi} - 3\ddot{\Phi} = 0. \quad (66)$$

VI. LATE-TIME DYNAMICS: EINSTEIN EQUATIONS

We are now at a stage to derive the Einstein equations. This study emphasizes the dynamics of the late-time Universe, where we can neglect the contribution

of radiation. We exclusively consider matter and dark energy, where 'matter' refers to cold dark matter and baryons combined. Henceforth, we use the abbreviation 'DE' for dark energy and denote any quantity related to dark energy with the subscript 'Q'. In this scenario, the Einstein equations are obtained perturbatively as follows

$$G_\nu^\mu = \frac{8\pi G}{c^4} [T_\nu^\mu(\text{matter}) + T_\nu^\mu(\text{DE})], \quad (67)$$

$$\bar{G}_\nu^\mu = \frac{8\pi G}{c^4} [\bar{T}_\nu^\mu(\text{matter}) + \bar{T}_\nu^\mu(\text{DE})], \quad (68)$$

$$\delta G_\nu^\mu = \frac{8\pi G}{c^4} [\delta T_\nu^\mu(\text{matter}) + \delta T_\nu^\mu(\text{DE})], \quad (69)$$

where G represents Newton's gravitational constant. Utilizing all the above equations, we finally obtain the two independent non-trivial Einstein equations for the background evolution, given below

$$3H^2 = 8\pi G(\bar{\rho}_m + \bar{\rho}_Q) - \frac{3c^2\kappa}{a^2}, \quad (70)$$

$$2\dot{H} + 3H^2 = -\frac{8\pi G}{c^2}\bar{P}_Q - \frac{c^2\kappa}{a^2}. \quad (71)$$

The t - t component of the first-order perturbation in the Einstein equations is given as

$$\begin{aligned} \frac{c^2(\vec{\nabla}^2\Phi + 3\kappa\Phi)}{a^2} - 3H(\dot{\Phi} + H\Phi) &= 4\pi G(\delta\rho_m + \delta\rho_Q) \\ &= 4\pi G(\bar{\rho}_m\delta_m + \bar{\rho}_Q\delta_Q). \end{aligned} \quad (72)$$

The three independent equations corresponding to the r - t (or t - r), θ - t (or t - θ), and ϕ - t (or t - ϕ) components of the first-order perturbation in the Einstein equations are given as

$$\frac{\partial B}{\partial r} = 0, \quad (73)$$

$$\frac{\partial B}{\partial \theta} = 0, \quad (74)$$

$$\frac{\partial B}{\partial \phi} = 0, \quad (75)$$

respectively, where we have

$$B = \dot{\Phi} + H\Phi - \frac{4\pi G a}{c^2} [\bar{\rho}_m v_m + \bar{\rho}_Q(1 + w_Q)v_Q]. \quad (76)$$

Eqs.(73), (74), and (75) can be manipulated to be written in a single equation, as

$$\frac{1}{h_r h_\theta h_\phi} \left[\frac{\partial}{\partial r} \left(\frac{h_\theta h_\phi}{h_r} \frac{\partial B}{\partial r} \right) + \frac{\partial}{\partial \theta} \left(\frac{h_\phi h_r}{h_\theta} \frac{\partial B}{\partial \theta} \right) + \frac{\partial}{\partial \phi} \left(\frac{h_r h_\theta}{h_\phi} \frac{\partial B}{\partial \phi} \right) \right] = \vec{\nabla}^2 B = 0. \quad (77)$$

Substituting the expression of B from Eq.(76) into Eq.(77), we finally obtain a simplified form of all three Einstein equations in a useful single equation, as

$$c^2 \vec{\nabla}^2 (\dot{\Phi} + H\Phi) = 4\pi G a [\bar{\rho}_m \theta_m + \bar{\rho}_Q (1 + w_Q) \theta_Q]. \quad (78)$$

Finally, a single independent equation from either the r -, θ -, or ϕ - ϕ components of the first-order perturbation in the Einstein equations is given as

$$\ddot{\Phi} + 4H\dot{\Phi} + (2\dot{H} + 3H^2)\Phi - \frac{c^2 \kappa \Phi}{a^2} = \frac{4\pi G}{c^2} \delta P_Q. \quad (79)$$

All other Einstein equations are trivially zero, so no additional equations arise.

VII. LATE-TIME DYNAMICS: SUB-HUBBLE APPROXIMATION

We are now focusing on sub-Hubble scales to study the evolution of perturbations, particularly matter density contrast. On sub-Hubble scales, we assume that the spatial derivatives of a quantity are significantly larger than its time derivative. Therefore, we can neglect the terms $H\dot{\Phi}$ and $\ddot{\Phi}$ compared to the term $\frac{c^2 \vec{\nabla}^2 \Phi}{a^2}$ in Eq.(66). Thus, in the sub-Hubble limit, Eq.(66) can be approximated as

$$\ddot{\delta}_m + 2H\dot{\delta}_m - \frac{c^2 \vec{\nabla}^2 \Phi}{a^2} \simeq 0. \quad (80)$$

Applying similar approximations, in the sub-Hubble limit, Eq.(72) can be approximated as

$$\frac{c^2 \vec{\nabla}^2 \Phi}{a^2} \simeq 4\pi G (\bar{\rho}_m \delta_m + \bar{\rho}_Q \delta_Q). \quad (81)$$

Now, by substituting Eq.(81) into Eq.(80), we obtain the evolution equation for the matter density contrast as

$$\begin{aligned} \ddot{\delta}_m + 2H\dot{\delta}_m &\simeq 4\pi G (\bar{\rho}_m \delta_m + \bar{\rho}_Q \delta_Q) \\ &= \frac{3}{2} H^2 (\Omega_m \delta_m + \Omega_Q \delta_Q), \end{aligned} \quad (82)$$

where we define the density parameters for curvature, matter, and dark energy as

$$\begin{aligned} \Omega_k &= -\frac{c^2 \kappa}{a^2 H^2}, \quad \Omega_m = \frac{8\pi G \bar{\rho}_m}{3H^2}, \\ \Omega_Q &= \frac{8\pi G \bar{\rho}_Q}{3H^2} = 1 - \Omega_m - \Omega_k. \end{aligned} \quad (83)$$

respectively. In the above equation, the last equality is a manifestation of Eq.(70). Utilizing the above definitions and expressing the derivatives w.r.t the e-fold, $N = \ln a$, Eq.(83) can be rewritten as

$$\frac{d^2 \delta_m}{dN^2} + F \frac{d\delta_m}{dN} - \frac{3}{2} [\Omega_m \delta_m + (1 - \Omega_m - \Omega_k) \delta_Q] \simeq 0, \quad (84)$$

where we have

$$\begin{aligned} F &= 2 + \frac{1}{H} \frac{dH}{dN} = 2 + \frac{\dot{H}}{H^2} \\ &= \frac{1}{2} [2 - \Omega_m - (1 + 3w_Q) (1 - \Omega_m - \Omega_k)]. \end{aligned} \quad (85)$$

A. Homogeneous dark energy

In this study, we focus on the homogeneous dark energy models, where dark energy has no fluctuations. Later, in the next study, we shall consider models in which the dark energy is not homogeneous. In the homogeneous dark energy models, we have $\delta_Q = 0$ and the evolution equation for the matter density contrast becomes

$$\begin{aligned} \frac{d^2 \delta_m}{dN^2} + \frac{1}{2} [2 - \Omega_m - (1 + 3w_Q) (1 - \Omega_m - \Omega_k)] \frac{d\delta_m}{dN} \\ - \frac{3}{2} \Omega_m \delta_m \simeq 0. \end{aligned} \quad (86)$$

Additionally, by solving Eq.(59) and employing the definitions in Eq.(83), we obtain

$$\Omega_m = \frac{\Omega_{m0} a^{-3}}{E^2} = \frac{\Omega_{m0} e^{-3N}}{E^2} = \frac{\Omega_{m0} (1+z)^3}{E^2}, \quad (87)$$

where E denotes the normalized Hubble parameter, defined as $E = \frac{H}{H_0}$, where H_0 represents the present value of the Hubble parameter. Ω_{m0} represents the present value of the matter density contrast. z represents the redshift and is related to the scale factor as $1+z = \frac{1}{a}$. The definition of Ω_k in Eq.(83) can be manipulated to be rewritten as

$$\Omega_k = \frac{\Omega_{k0}a^{-2}}{E^2} = \frac{\Omega_{k0}e^{-2N}}{E^2} = \frac{\Omega_{k0}(1+z)^2}{E^2}, \quad (88)$$

where Ω_{k0} denotes the present value of the curvature density contrast. By employing Eqs.(87) and (88), along with the background Einstein equation Eq.(70), the normalized Hubble parameter E can be expressed as

$$E^2 = \Omega_{m0}(1+z)^3 + \Omega_{k0}(1+z)^2 + (1 - \Omega_{m0} - \Omega_{k0})f_{DE}, \quad (89)$$

where f_{DE} is connected to the evolution of dark energy density and can be computed from the expression of the equation of state of dark energy, w_Q , as given below

$$f_{DE} = \exp \left[3 \int_0^z \frac{1 + w_Q(\tilde{z})}{1 + \tilde{z}} d\tilde{z} \right], \quad (90)$$

where \tilde{z} serves as the dummy variable for the redshift z . In this study, we exclusively focus on three prominent dark energy models, namely the parametrizations of the equation of state of dark energy w_Q : the Λ CDM model, the w CDM parametrization, and the Chevallier-Polarski-Linder (CPL) parametrization [77, 78]. In these parametrizations, the equation of state for dark energy is expressed as

$$w_Q (\Lambda\text{CDM}) = -1, \quad (91)$$

$$w_Q (w\text{CDM}) = w_0, \quad (92)$$

$$w_Q (\text{CPL}) = w_0 + w_a \frac{z}{1+z}, \quad (93)$$

respectively, where w_0 serves as the model parameter for the w CDM model, while w_0 and w_a are the two model parameters for the CPL parametrization. Therefore, the w CDM model is a subset of the CPL model where $w_a = 0$. The Λ CDM model is a subset of the CPL model where $w_0 = -1$ and $w_a = 0$, and it is also a subset of the w CDM model where $w_0 = -1$. By substituting Eqs.(91), (92), and (93) into Eq.(90), we obtain the expressions of f_{DE} for the Λ CDM, the w CDM, and the CPL models

$$f_{DE} (\Lambda\text{CDM}) = 1, \quad (94)$$

$$f_{DE} (w\text{CDM}) = (1+z)^{3(1+w_0)}, \quad (95)$$

$$f_{DE} (\text{CPL}) = (1+z)^{3(1+w_0+w_a)} e^{-3w_a \frac{z}{1+z}}, \quad (96)$$

respectively.

B. Initial conditions

We consider initial conditions in the early matter-dominated era to solve the differential equation in Eq.(86) at an initial redshift $z^i = 1100$. We denote the initial value of any quantity by the superscript "i". In the matter-dominated era, we approximately have $\Omega_m \simeq 1$, $\Omega_k \simeq 0$, and $\Omega_Q \simeq 0$. With these approximations, the evolution equation for δ_m during the matter-dominated era becomes

$$\frac{d^2 \delta_m}{dN^2} + \frac{1}{2} \frac{d\delta_m}{dN} - \frac{3}{2} \delta_m \simeq 0$$

(at early matter dominated era). (97)

There are two solutions to the above differential equation. One is proportional to $a^{-3/2}$, representing the decaying solution. The other is the growing solution, corresponding to $\delta_m \propto a$. As we are interested in the growing mode solutions, we set the initial conditions accordingly as

$$\delta_m^i = a^i, \quad (98)$$

$$\left(\frac{d\delta_m}{dN} \right)^i = a^i. \quad (99)$$

C. f and σ_8

We are now turning our attention to two additional quantities. The first one is the logarithmic growth factor, defined as [87]

$$f = \frac{d \ln D_+}{d \ln a}, \quad (100)$$

where D_+ represents the growing mode solution of the matter density contrast, δ_m . In the sub-Hubble limit within this framework, the normalization factor of the matter power spectrum, denoted as σ_8 , retains its scale-independence and can be represented as [88]

IX. RESULTS

$$\sigma_8(z) = \sigma_{80} \frac{D_+(z)}{D_+(z=0)}, \quad (101)$$

where σ_{80} denotes the present value of σ_8 .

VIII. OBSERVATIONAL DATA

In our analysis, we incorporate diverse observational datasets to robustly constrain the model parameters and cosmological nuisance parameters. We consider the Pantheon compilation, which compiles type Ia supernova observations. These supernovae serve as standard candles, and their apparent peak absolute magnitudes vary with redshift [7]. The observed apparent magnitude is dependent on both the luminosity of the source at a given redshift and the nuisance parameter M_B , representing the peak absolute magnitude of a type Ia supernova. We additionally take into account the covariances existing between data points at varying redshifts. To ensure a comprehensive analysis, we label this dataset as 'SN'.

We consider data from cosmic chronometer (CC) observations with 32 Hubble parameter measurements spanning a diverse range of redshift values ($0.07 \leq z \leq 1.965$) [17]. Note that, within these 32 Hubble parameter measurements, 15 data points have correlations among themselves and we incorporate these into our analysis. We denote this dataset as 'CC'.

We also consider baryon acoustic oscillations (BAO) data in our analysis. These observations provide insights into cosmological distances, specifically the angular diameter distance. The BAO dataset includes measurements in both the line of sight and transverse directions [13]. The former is connected to the Hubble parameter, while the latter is linked to the angular diameter distance [12–14]. For the BAO data, we closely follow Alam et al. 2021 [13], except eBOSS emission-line galaxies (ELGs) data at $z = 0.8$ due to asymmetric standard deviations. We label the BAO observations as 'BAO'. Notably, BAO measurements are sensitive to the parameter r_d , representing the distance to the baryon drag epoch. We treat r_d as a nuisance parameter in our analysis.

Finally, we consider $f\sigma_8$ data, spanning redshifts from $z = 0.001$ to $z = 1.944$, to constrain the model parameters across both background and perturbation evolutions [89]. This dataset is labeled as ' $f\sigma_8$ '.

Using the above-mentioned observational data, we constrain all the model parameters in all three dark energy models. In Figure 1, a triangle plot is presented to display the confidence contours of each pair of parameters and the marginal probability plots for each parameter in the Λ CDM model. The black lines represent the 'CC+BAO+SN+ $f\sigma_8$ ' combination of the dataset, where cosmic curvature is taken into account in the analysis. The blue lines correspond to the 'CC+BAO+SN' combination of the dataset, incorporating cosmic curvature. The green lines depict the 'CC+BAO+SN+ $f\sigma_8$ ' combination of the dataset, but in this case, cosmic curvature is not considered in the analysis (i.e., $\Omega_{k0} = 0$). The same color combinations are maintained for the same cases in the other two figures.

It is noteworthy that in all the figures, a quantity h is considered, which is related to H_0 and given as

$$H_0 = 100 h \text{ km s}^{-1} \text{ Mpc}^{-1}. \quad (102)$$

We present all the marginalized 1σ bounds on the parameters of the Λ CDM model in Table I. Examining Figure 1 and Table I, it is evident that the marginalized bounds on h , r_d , and M_B remain similar in all three cases. This suggests that the inclusion of $f\sigma_8$ data or the consideration of cosmic curvature in the analysis does not significantly alter the constraints on these parameters.

The constraints on Ω_{k0} also exhibit similarity between the 'CC+BAO+SN+ $f\sigma_8$ ' and 'CC+BAO+SN' combinations. This implies that the inclusion of $f\sigma_8$ data does not lead to notable improvements in constraining the Ω_{k0} parameter. Notably, interesting results emerge in the constraints on the Ω_{m0} and σ_{80} parameters. Constraints on Ω_{m0} are similar for both 'CC+BAO+SN+ $f\sigma_8$ ' and 'CC+BAO+SN' combinations but become notably tighter when cosmic curvature is excluded, i.e., for 'CC+BAO+SN+ $f\sigma_8$ (flat)' (green line) combination. Similarly, the constraint on the σ_{80} parameter is significantly tighter when the contribution of cosmic curvature is excluded. Furthermore, not only is the constraint tighter, but the mean value of σ_{80} is higher when cosmic curvature is included in the analysis.

In Figure 2, we present triangle plots illustrating the w CDM model parameters for the same combinations of datasets, maintaining consistent color codes as in Figure 1. Corresponding 1σ bounds on the w CDM model parameters are tabulated in Table II. Notably, an additional parameter, w_0 , is introduced compared to the

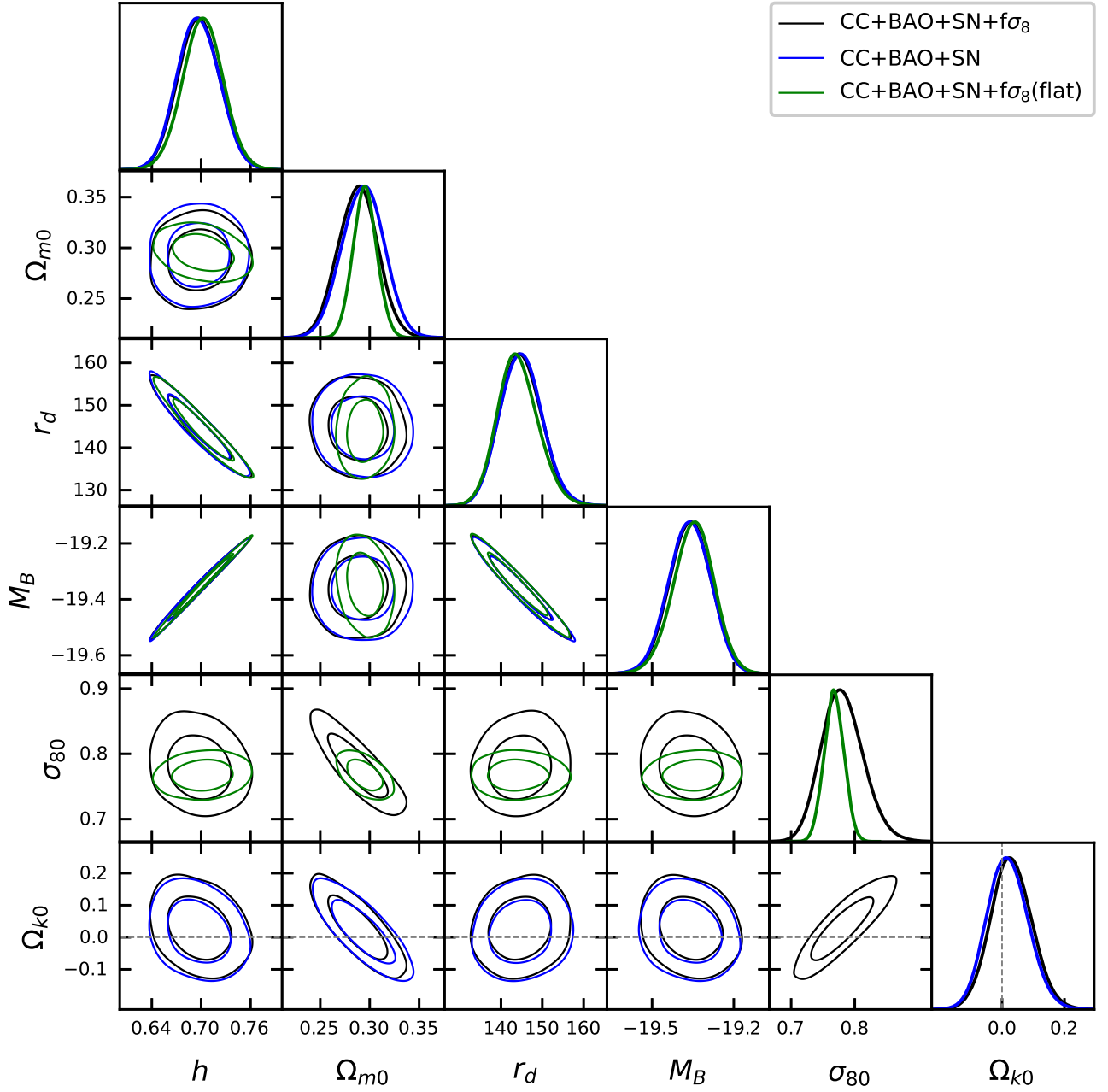


FIG. 1: Constraints on the parameters of the Λ CDM model are depicted through various contour lines and marginalized probabilities through a triangle plot. The black, blue, and green lines correspond to the dataset combinations 'CC+BAO+SN+ $f\sigma_8$ ' (considering cosmic curvature), 'CC+BAO+SN' (considering cosmic curvature), and 'CC+BAO+SN+ $f\sigma_8$ (flat)' (excluding cosmic curvature), respectively.

Λ CDM model. Similar to the Λ CDM model, the bounds on h , r_d , and M_B exhibit similarity across all three cases.

For Ω_{m0} and σ_{80} parameters, constraints are marginally tighter in the flat case compared to the non-flat cases, although not significantly so. The Λ CDM model, corresponding to $w_0 = -1$, is almost 1σ away from the mean values obtained in all three cases. No-

tably, the non-phantom behavior ($w_0 > -1$) of dark energy appears more favorable compared to the phantom behavior ($w_0 < -1$) in all three cases.

In Figure 3, we present triangle plots illustrating the CPL model parameters for the same combinations of datasets, maintaining consistent color codes as in Figures 1 and 2. Corresponding 1σ bounds on the CPL

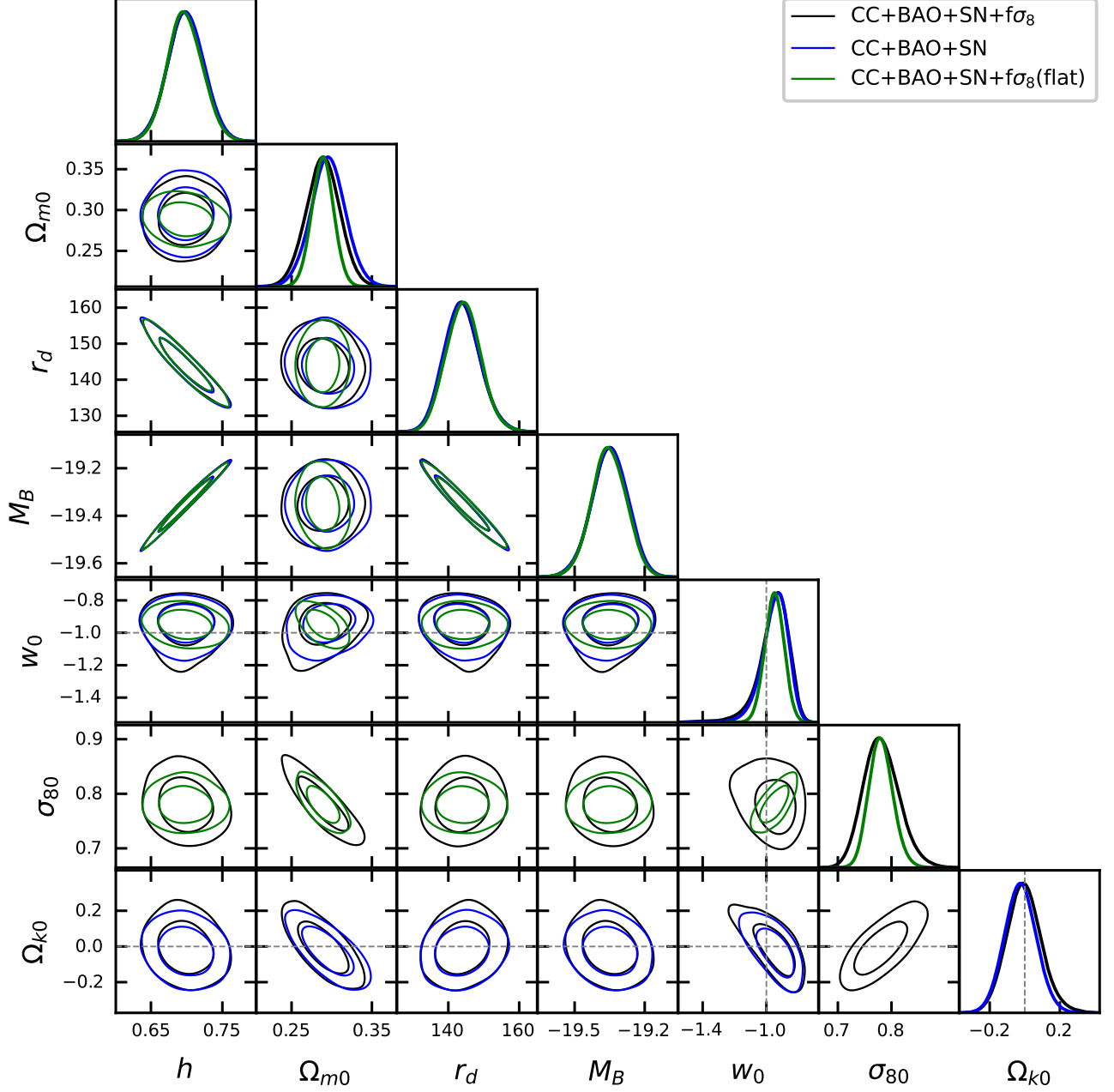


FIG. 2: The constraints on the parameters of the w CDM model are illustrated through different contour lines and marginalized probabilities through a triangle plot. The black, blue, and green lines correspond to the dataset combinations ‘CC+BAO+SN+ $f\sigma_8$ ’ (including cosmic curvature), ‘CC+BAO+SN’ (including cosmic curvature), and ‘CC+BAO+SN+ $f\sigma_8$ (flat)’ (excluding cosmic curvature), respectively.

model parameters are tabulated in Table III. Similar to the Λ CDM and w CDM models, the bounds on h , r_d , and M_B remain similar across all three cases.

In contrast to the previous two models, the CPL model exhibits nearly identical bounds on the σ_{80} parameter in both flat and non-flat cases. Moreover, for the Ω_{m0} parameter, the CPL model displays a different be-

havior in constraints compared to the previous two models. The constraints on Ω_{m0} are similar in both flat and non-flat cases, but excluding $f\sigma_8$ data results in looser constraints, with the mean value being comparatively lower.

Constraints on w_0 and w_a parameters are similar across all three combinations. Similar to the w CDM

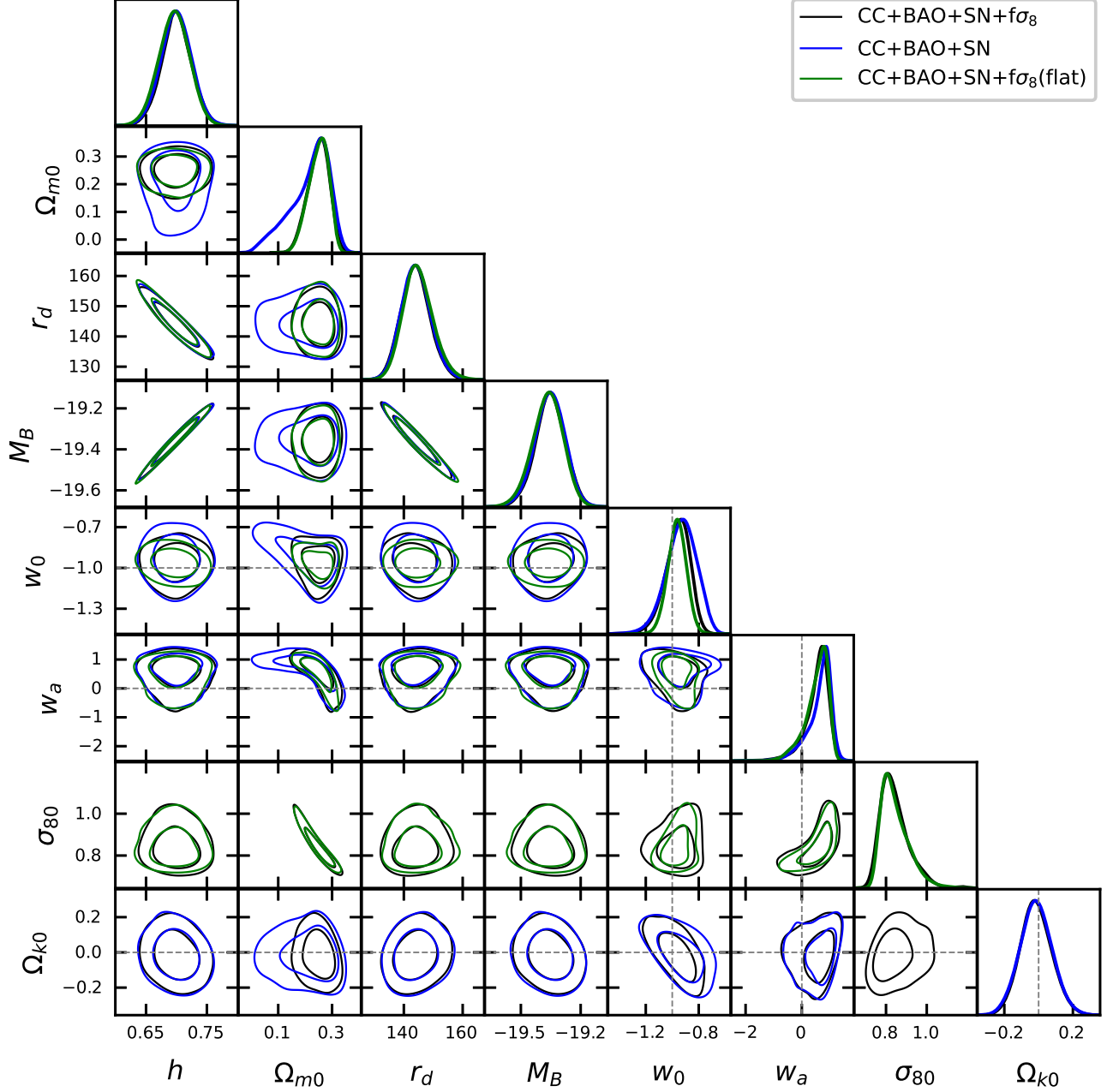


FIG. 3: The constraints on the parameters of the CPL model are depicted through various contour lines and marginalized probabilities through a triangle plot. The black, blue, and green lines correspond to the dataset combinations ‘CC+BAO+SN+ $f\sigma_8$ ’ (considering cosmic curvature), ‘CC+BAO+SN’ (considering cosmic curvature), and ‘CC+BAO+SN+ $f\sigma_8$ (flat)’ (excluding cosmic curvature), respectively.

model, in the CPL model, we find that the Λ CDM model, representing $w_0 = -1$ and $w_a = 0$, is almost 1σ away from the mean values obtained in all three cases. Similar to the w CDM model, here also, the non-phantom behavior ($w_0 > -1$ and $w_a > 0$) of dark energy appears more favorable compared to the phantom behavior ($w_0 < -1$ and $w_a < 0$) in all three cases.

X. CONCLUSION

We delve into the impact of cosmic curvature on structure formation through a comprehensive analysis utilizing general relativistic first-order perturbation theory within the Newtonian gauge. This investigation specifically focuses on scalar fluctuations and excludes

Parameters	CC+BAO+SN+ $f\sigma_8$	CC+BAO+SN	CC+BAO+SN+ $f\sigma_8$ (flat)
h	0.698 ± 0.025	0.696 ± 0.025	0.702 ± 0.024
Ω_{m0}	0.288 ± 0.020	0.293 ± 0.021	0.295 ± 0.012
r_d	144.7 ± 5.0	144.9 ± 5.0	$144.1^{+4.4}_{-5.2}$
M_B	-19.359 ± 0.076	-19.362 ± 0.076	-19.348 ± 0.075
σ_{80}	$0.781^{+0.029}_{-0.035}$	–	0.767 ± 0.016
Ω_{k0}	0.030 ± 0.065	$0.018^{+0.061}_{-0.068}$	–

TABLE I: 1σ bounds on the parameters of the Λ CDM model corresponding to three different combinations of datasets mentioned in the table.

Parameters	CC+BAO+SN+ $f\sigma_8$	CC+BAO+SN	CC+BAO+SN+ $f\sigma_8$ (flat)
h	0.698 ± 0.025	0.699 ± 0.025	0.698 ± 0.025
Ω_{m0}	0.289 ± 0.021	0.295 ± 0.021	0.289 ± 0.014
r_d	$144.1^{+4.6}_{-5.1}$	$143.9^{+4.6}_{-5.4}$	144.3 ± 4.9
M_B	-19.350 ± 0.076	-19.350 ± 0.077	-19.353 ± 0.074
w_0	$-0.956^{+0.11}_{-0.063}$	$-0.947^{+0.091}_{-0.064}$	-0.950 ± 0.060
σ_{80}	$0.781^{+0.030}_{-0.036}$	–	$0.781^{+0.021}_{-0.024}$
Ω_{k0}	-0.004 ± 0.099	-0.025 ± 0.090	–

TABLE II: 1σ bounds on the parameters of the w CDM model corresponding to three different combinations of datasets mentioned in the table.

any source of anisotropic stress.

Our computations involve continuity and Euler equations for a general fluid, as well as Einstein equations that incorporate cosmic curvature. Emphasizing the late-time dynamics of background expansion and first-order fluctuations, we scrutinize the evolution of matter density contrast in the presence of cosmic curvature and dark energy perturbations. While we have developed perturbation equations considering cosmic curvature and dark energy perturbations, our current application narrows its focus to the influence of cosmic curvature on the large-scale structure formation with the homogeneous dark energy models. We explore this aspect with three distinct dark energy models Λ CDM, w CDM, and CPL, reserving the inclusion of dark energy perturbations for future studies.

We rewrite the evolution of matter density contrast considering cosmic curvature and dark energy perturbations on the sub-Hubble scales using sub-Hubble assumptions. Employing proper initial conditions, we solve the evolution equation and conduct data analysis using four key observational datasets: cosmic chronome-

ters (CC), baryon acoustic oscillations (BAO), type Ia supernova observations (SN), and $f\sigma_8$ data.

We find that constraints on parameters like h (or H_0), r_d , and M_B remain largely unaffected by the inclusion of cosmic curvature or the presence of growth data ($f\sigma_8$) across all three models considered in this analysis. However, in the case of Ω_{m0} and σ_{80} parameters, exclusion of cosmic curvature tightens constraints on Ω_{m0} and σ_{80} in Λ CDM and w CDM models compared to their non-flat counterparts. In contrast, for the CPL model, constraints on σ_{80} remain consistent in all cases, while constraints on Ω_{m0} are tighter, with a higher mean value when incorporating $f\sigma_8$ data, regardless of cosmic curvature.

Notably, in both w CDM and CPL models, the Λ CDM model stands almost 1σ away from the mean values obtained from data analysis for all data combinations. Moreover, the non-phantom behavior of dark energy emerges as more favorable than the phantom behavior in both models and across all data combinations.

Parameters	CC+BAO+SN+ $f\sigma_8$	CC+BAO+SN	CC+BAO+SN+ $f\sigma_8$ (flat)
h	0.700 ± 0.024	0.699 ± 0.025	0.696 ± 0.025
Ω_{m0}	$0.249^{+0.044}_{-0.034}$	$0.217^{+0.092}_{-0.043}$	$0.249^{+0.044}_{-0.032}$
r_d	$144.0^{+4.5}_{-5.1}$	$144.2^{+4.5}_{-5.3}$	$144.9^{+4.5}_{-5.5}$
M_B	-19.353 ± 0.074	$-19.355^{+0.078}_{-0.071}$	$-19.365^{+0.081}_{-0.071}$
w_0	$-0.961^{+0.11}_{-0.077}$	$-0.93^{+0.12}_{-0.10}$	-0.964 ± 0.071
w_a	$0.54^{+0.47}_{-0.22}$	$0.63^{+0.50}_{-0.20}$	$0.53^{+0.50}_{-0.22}$
σ_{80}	$0.843^{+0.043}_{-0.084}$	–	$0.845^{+0.039}_{-0.083}$
Ω_{k0}	-0.015 ± 0.092	-0.015 ± 0.094	–

TABLE III: 1σ bounds on the parameters of the CPL model corresponding to three different combinations of datasets mentioned in the table.

Acknowledgements

The author would like to acknowledge IISER Kolkata for its financial support through the postdoctoral

fellowship. The revision for this work was carried out during the author's tenure at UWC, partially supported by the South African Radio Astronomy Observatory and National Research Foundation (Grant No. 75415).

-
- [1] S. Perlmutter et al. (Supernova Cosmology Project), *Nature* **391**, 51 (1998), [arXiv:astro-ph/9712212](#) .
- [2] A. G. Riess et al. (Supernova Search Team), *Astron. J.* **116**, 1009 (1998), [arXiv:astro-ph/9805201](#) .
- [3] S. Perlmutter et al. (Supernova Cosmology Project), *Astrophys. J.* **517**, 565 (1999), [arXiv:astro-ph/9812133](#) .
- [4] A. Wright, *Nature Physics* **7**, 833 (2011).
- [5] S. Linden, J. M. Virey, and A. Tilquin, *Astronomy and Astrophysics* **506**, 1095 (2009).
- [6] D. Camarena and V. Marra, *Mon. Not. Roy. Astron. Soc.* **495**, 2630 (2020), [arXiv:1910.14125 \[astro-ph.CO\]](#) .
- [7] D. M. Scolnic et al. (Pan-STARRS1), *Astrophys. J.* **859**, 101 (2018), [arXiv:1710.00845 \[astro-ph.CO\]](#) .
- [8] A. K. Çamlıbel, I. Semiz, and M. A. Feyizoglu, *Class. Quant. Grav.* **37**, 235001 (2020), [arXiv:2001.04408 \[astro-ph.CO\]](#) .
- [9] P. A. R. Ade et al. (Planck), *Astron. Astrophys.* **571**, A16 (2014), [arXiv:1303.5076 \[astro-ph.CO\]](#) .
- [10] P. A. R. Ade et al. (Planck), *Astron. Astrophys.* **594**, A13 (2016), [arXiv:1502.01589 \[astro-ph.CO\]](#) .
- [11] N. Aghanim et al. (Planck), *Astron. Astrophys.* **641**, A6 (2020), [Erratum: *Astron. Astrophys.* 652, C4 (2021)], [arXiv:1807.06209 \[astro-ph.CO\]](#) .
- [12] S. Alam et al. (BOSS), *Mon. Not. Roy. Astron. Soc.* **470**, 2617 (2017), [arXiv:1607.03155 \[astro-ph.CO\]](#) .
- [13] S. Alam et al. (eBOSS), *Phys. Rev. D* **103**, 083533 (2021), [arXiv:2007.08991 \[astro-ph.CO\]](#) .
- [14] J. Hou et al., *Mon. Not. Roy. Astron. Soc.* **500**, 1201 (2020), [arXiv:2007.08998 \[astro-ph.CO\]](#) .
- [15] R. Jimenez and A. Loeb, *Astrophys. J.* **573**, 37 (2002), [arXiv:astro-ph/0106145](#) .
- [16] A. M. Pinho, S. Casas, and L. Amendola, *JCAP* **11**, 027 (2018), [arXiv:1805.00027 \[astro-ph.CO\]](#) .
- [17] S. Cao and B. Ratra, *Phys. Rev. D* **107**, 103521 (2023), [arXiv:2302.14203 \[astro-ph.CO\]](#) .
- [18] P. J. E. Peebles and B. Ratra, *Rev. Mod. Phys.* **75**, 559 (2003), [arXiv:astro-ph/0207347](#) .
- [19] E. J. Copeland, M. Sami, and S. Tsujikawa, *Int. J. Mod. Phys. D* **15**, 1753 (2006), [arXiv:hep-th/0603057](#) .
- [20] J. Yoo and Y. Watanabe, *Int. J. Mod. Phys. D* **21**, 1230002 (2012), [arXiv:1212.4726 \[astro-ph.CO\]](#) .
- [21] A. I. Lonappan, S. Kumar, Ruchika, B. R. Dinda, and A. A. Sen, *Phys. Rev. D* **97**, 043524 (2018), [arXiv:1707.00603 \[astro-ph.CO\]](#) .
- [22] B. R. Dinda, *JCAP* **09**, 035 (2017), [arXiv:1705.00657 \[astro-ph.CO\]](#) .
- [23] B. R. Dinda, A. A. Sen, and T. R. Choudhury, (2018), [arXiv:1804.11137 \[astro-ph.CO\]](#) .
- [24] T. Clifton, P. G. Ferreira, A. Padilla, and C. Skordis, *Phys. Rept.* **513**, 1 (2012),

- arXiv:1106.2476 [astro-ph.CO] .
- [25] K. Koyama, *Rept. Prog. Phys.* **79**, 046902 (2016), arXiv:1504.04623 [astro-ph.CO] .
- [26] S. Tsujikawa, *Lect. Notes Phys.* **800**, 99 (2010), arXiv:1101.0191 [gr-qc] .
- [27] A. Joyce, L. Lombriser, and F. Schmidt, *Ann. Rev. Nucl. Part. Sci.* **66**, 95 (2016), arXiv:1601.06133 [astro-ph.CO] .
- [28] B. R. Dinda, M. Wali Hossain, and A. A. Sen, *JCAP* **01**, 045 (2018), arXiv:1706.00567 [astro-ph.CO] .
- [29] B. R. Dinda, *JCAP* **06**, 017 (2018), arXiv:1801.01741 [astro-ph.CO] .
- [30] J. Zhang, B. R. Dinda, M. W. Hossain, A. A. Sen, and W. Luo, *Phys. Rev. D* **102**, 043510 (2020), arXiv:2004.12659 [astro-ph.CO] .
- [31] B. R. Dinda, M. W. Hossain, and A. A. Sen, *J. Astrophys. Astron.* **44**, 85 (2023), arXiv:2208.11560 [astro-ph.CO] .
- [32] A. Bassi, B. R. Dinda, and A. A. Sen, *J. Astrophys. Astron.* **44**, 93 (2023), arXiv:2306.03875 [astro-ph.CO] .
- [33] S. Nojiri and S. D. Odintsov, *Phys. Rept.* **505**, 59 (2011), arXiv:1011.0544 [gr-qc] .
- [34] S. Nojiri, S. D. Odintsov, and V. K. Oikonomou, *Phys. Rept.* **692**, 1 (2017), arXiv:1705.11098 [gr-qc] .
- [35] K. Bamba, S. Capozziello, S. Nojiri, and S. D. Odintsov, *Astrophys. Space Sci.* **342**, 155 (2012), arXiv:1205.3421 [gr-qc] .
- [36] B.-H. Lee, W. Lee, E. O. Colgáin, M. M. Sheikh-Jabbari, and S. Thakur, *JCAP* **04**, 004 (2022), arXiv:2202.03906 [astro-ph.CO] .
- [37] S. M. Carroll, *Living Rev. Rel.* **4**, 1 (2001), arXiv:astro-ph/0004075 .
- [38] I. Zlatev, L.-M. Wang, and P. J. Steinhardt, *Phys. Rev. Lett.* **82**, 896 (1999), arXiv:astro-ph/9807002 .
- [39] V. Sahni and A. A. Starobinsky, *Int. J. Mod. Phys. D* **9**, 373 (2000), arXiv:astro-ph/9904398 .
- [40] H. Velten, R. vom Marttens, and W. Zimdahl, *Eur. Phys. J. C* **74**, 3160 (2014), arXiv:1410.2509 [astro-ph.CO] .
- [41] M. Malquarti, E. J. Copeland, and A. R. Liddle, *Phys. Rev. D* **68**, 023512 (2003), arXiv:astro-ph/0304277 .
- [42] E. Di Valentino, O. Mena, S. Pan, L. Visinelli, W. Yang, A. Melchiorri, D. F. Mota, A. G. Riess, and J. Silk, *Class. Quant. Grav.* **38**, 153001 (2021), arXiv:2103.01183 [astro-ph.CO] .
- [43] C. Krishnan, R. Mohayaee, E. O. Colgáin, M. M. Sheikh-Jabbari, and L. Yin, *Class. Quant. Grav.* **38**, 184001 (2021), arXiv:2105.09790 [astro-ph.CO] .
- [44] S. Vagnozzi, *Phys. Rev. D* **102**, 023518 (2020), arXiv:1907.07569 [astro-ph.CO] .
- [45] B. R. Dinda, *Phys. Rev. D* **105**, 063524 (2022), arXiv:2106.02963 [astro-ph.CO] .
- [46] E. Di Valentino et al., *Astropart. Phys.* **131**, 102604 (2021), arXiv:2008.11285 [astro-ph.CO] .
- [47] E. Abdalla et al., *JHEAp* **34**, 49 (2022), arXiv:2203.06142 [astro-ph.CO] .
- [48] M. Douspis, L. Salvati, and N. Aghanim, *PoS EDSU2018*, 037 (2018), arXiv:1901.05289 [astro-ph.CO] .
- [49] A. Bhattacharyya, U. Alam, K. L. Pandey, S. Das, and S. Pal, *Astrophys. J.* **876**, 143 (2019), arXiv:1805.04716 [astro-ph.CO] .
- [50] W. Handley, *Phys. Rev. D* **103**, L041301 (2021), arXiv:1908.09139 [astro-ph.CO] .
- [51] C. Desgrange, A. Heinesen, and T. Buchert, *Int. J. Mod. Phys. D* **28**, 1950143 (2019), arXiv:1902.07915 [astro-ph.CO] .
- [52] A. Coley and G. Ellis, *Class. Quant. Grav.* **37**, 013001 (2020), arXiv:1909.05346 [gr-qc] .
- [53] E. Di Valentino et al., *Astropart. Phys.* **131**, 102607 (2021), arXiv:2008.11286 [astro-ph.CO] .
- [54] M. Moresco, R. Jimenez, L. Verde, A. Cimatti, L. Pozzetti, C. Maraston, and D. Thomas, *JCAP* **12**, 039 (2016), arXiv:1604.00183 [astro-ph.CO] .
- [55] J.-J. Wei and X.-F. Wu, *Astrophys. J.* **838**, 160 (2017), arXiv:1611.00904 [astro-ph.CO] .
- [56] G.-J. Wang, J.-J. Wei, Z.-X. Li, J.-Q. Xia, and Z.-H. Zhu, *Astrophys. J.* **847**, 45 (2017), arXiv:1709.07258 [astro-ph.CO] .
- [57] C.-Z. Ruan, F. Melia, Y. Chen, and T.-J. Zhang, *Astrophys. J.* **881**, 137 (2019), arXiv:1901.06626 [astro-ph.CO] .
- [58] Y. Yang and Y. Gong, *Mon. Not. Roy. Astron. Soc.* **504**, 3092 (2021), arXiv:2007.05714 [astro-ph.CO] .
- [59] S.-Y. Li, Y.-L. Li, T.-J. Zhang, and T. Zhang, *The Astrophysical Journal* **887**, 36 (2019).
- [60] B. Wang, J.-Z. Qi, J.-F. Zhang, and X. Zhang, *Astrophys. J.* **898**, 100 (2020), arXiv:1910.12173 [astro-ph.CO] .
- [61] B. R. Dinda, H. Singirikonda, and S. Majumdar, (2023), arXiv:2303.15401 [astro-ph.CO] .
- [62] H. Yu and F. Wang, *Astrophys. J.* **828**, 85 (2016), arXiv:1605.02483 [astro-ph.CO] .
- [63] J.-J. Wei and F. Melia, *The Astrophysical Journal* **888**, 99 (2020).
- [64] Y. Liu, S. Cao, T. Liu, X. Li, S. Geng, Y. Lian, and W. Guo, *Astrophys. J.* **901**, 129 (2020), arXiv:2008.08378 [astro-ph.CO] .
- [65] P. Mukherjee and N. Banerjee, *Phys. Rev. D* **105**, 063516 (2022), arXiv:2202.07886 [astro-ph.CO] .
- [66] J. Shi, *Eur. Phys. J. C* **83**, 951 (2023), arXiv:2307.08103 [gr-qc] .
- [67] S. Vagnozzi, A. Loeb, and M. Moresco, *Astrophys. J.* **908**, 84 (2021), arXiv:2011.11645 [astro-ph.CO] .

- [68] S. Dhawan, J. Alsing, and S. Vagnozzi, *Mon. Not. Roy. Astron. Soc.* **506**, L1 (2021), [arXiv:2104.02485 \[astro-ph.CO\]](#) .
- [69] W. Yang, W. Giarè, S. Pan, E. Di Valentino, A. Melchiorri, and J. Silk, *Phys. Rev. D* **107**, 063509 (2023), [arXiv:2210.09865 \[astro-ph.CO\]](#) .
- [70] J. Bel, J. Larena, R. Maartens, C. Marinoni, and L. Perenon, *JCAP* **09**, 076 (2022), [arXiv:2206.03059 \[astro-ph.CO\]](#) .
- [71] M. Eingorn, A. Emrah Yükselci, and A. Zhuk, *Eur. Phys. J. C* **79**, 655 (2019), [arXiv:1905.09502 \[gr-qc\]](#) .
- [72] C. Clarkson, M. Cortes, and B. A. Bassett, *JCAP* **08**, 011 (2007), [arXiv:astro-ph/0702670](#) .
- [73] C. Gao, Y. Chen, and J. Zheng, *Research in Astronomy and Astrophysics* **20**, 151 (2020).
- [74] Y. Wang and P. Mukherjee, *Phys. Rev. D* **76**, 103533 (2007), [arXiv:astro-ph/0703780](#) .
- [75] Y. Gong, Q. Wu, and A. Wang, *Astrophys. J.* **681**, 27 (2008), [arXiv:0708.1817 \[astro-ph\]](#) .
- [76] P. M. M. Alonso, C. Escamilla-Rivera, and R. Sandoval-Orozco, *JCAP* **04**, 084 (2024), [arXiv:2309.12292 \[astro-ph.CO\]](#) .
- [77] M. Chevallier and D. Polarski, *Int. J. Mod. Phys. D* **10**, 213 (2001), [arXiv:gr-qc/0009008](#) .
- [78] E. V. Linder, *Phys. Rev. Lett.* **90**, 091301 (2003), [arXiv:astro-ph/0208512](#) .
- [79] R. de Putter, D. Huterer, and E. V. Linder, *Phys. Rev. D* **81**, 103513 (2010).
- [80] R. C. Batista, *Universe* **8**, 22 (2021), [arXiv:2204.12341 \[astro-ph.CO\]](#) .
- [81] K. Bamba, J. Matsumoto, and S. Nojiri, *Phys. Rev. D* **85**, 084026 (2012), [arXiv:1109.1308 \[hep-th\]](#) .
- [82] J. Matsumoto, *Universe* **1**, 17 (2015), [arXiv:1401.3077 \[astro-ph.CO\]](#) .
- [83] B. R. Dinda, *J. Astrophys. Astron.* **40**, 12 (2019), [arXiv:1804.07953 \[astro-ph.CO\]](#) .
- [84] H. K. Jassal, J. S. Bagla, and T. Padmanabhan, *Phys. Rev. D* **72**, 103503 (2005), [arXiv:astro-ph/0506748](#) .
- [85] J. S. Bagla and T. Padmanabhan, *J. Astrophys. Astron.* **16**, 77 (1995), [arXiv:gr-qc/9309022](#) .
- [86] H. K. Jassal, J. S. Bagla, and T. Padmanabhan, *Mon. Not. Roy. Astron. Soc.* **356**, L11 (2005), [arXiv:astro-ph/0404378](#) .
- [87] D. Huterer *et al.*, *Astropart. Phys.* **63**, 23 (2015), [arXiv:1309.5385 \[astro-ph.CO\]](#) .
- [88] E. Pierpaoli, D. Scott, and M. J. White, *Mon. Not. Roy. Astron. Soc.* **325**, 77 (2001), [arXiv:astro-ph/0010039](#) .
- [89] L. Kazantzidis and L. Perivolaropoulos, *Phys. Rev. D* **97**, 103503 (2018), [arXiv:1803.01337 \[astro-ph.CO\]](#) .